Mon. Not. R. Astron. Soc. **000**, 1–14 (2012) Printed 6 June 2014 (MN LATEX style file v2.2)

A Multiwavelength Consensus on the Main Sequence of Star-Forming Galaxies at $z \sim 2$

G. Rodighiero[(1)⋆], A. Renzini[(2)], E. Daddi[(3)], I. Baronchelli[(1)], S. Berta[(4)], G. Cresci[(5)], A. Franceschini[(1)], C. Gruppioni[(6)], D. Lutz[(4)], C. Mancini[(2)], P. Santini[(7)], G. Zamorani[(6)], J. Silverman [(8)], D. Kashino[(9)], P. Andreani[(10)], A. Cimatti[(11)], H. Domínguez Sánchez[(12)], E. Le Floch[(3)], B. Magnelli[(4,13)], P. Popesso[(4)], F. Pozzi[(11)]

[(1)] *Dipartimento di Fisica e Astronomia, Università di Padova, vicolo dell'Osservatorio 3, I–35122 Padova, Italy.*
[(2)] *INAF - Osservatorio Astronomico di Padova, vicolo dell'Osservatorio 5, I-35122 Padova, Italy.*
[(3)] *CEA-Saclay, Service d'Astrophysique, F-91191 Gif-sur-Yvette, France.*
[(4)] *Max-Planck-Institut für Extraterrestrische Physik (MPE), Postfach 1312, D-85741 Garching, Germany.*
[(5)] *INAF - Osservatorio Astronomico di Arcetri, largo E. Fermi 5, I-50127 Firenze, Italy.*
[(6)] *INAF - Osservatorio Astronomico di Bologna, via Ranzani 1, I-40127 Bologna, Italy.*
[(7)] *INAF - Osservatorio Astronomico di Roma, via di Frascati 33, I-00040 Monte Porzio Catone, Italy.*
[(8)] *Kavli Institute for the Physics and Mathematics of the Universe (WPI), Todai Institutes for Advanced Study, The University of Tokyo, Kashiwanoha, Kashiwa 277-8583, Japan.*
[(9)] *Division of Particle and Astrophysical Science, Graduate School of Science, Nagoya University, Nagoya 464-8602, Japan.*
[(10)] *ESO, Karl-Schwarzschild-Strasse 2, D-85748 Garching, Germany.*
[(11)] *University of Bologna, Department of Physics and Astronomy (DIFA), V.le Berti Pichat, 6/2 - 40127, Bologna, Italy.*
[(12)] *Departamento de Astrofísica, Facultad de CC. and Físicas, Universidad Complutense de Madrid, E-28040, Madrid, Spain.*
[(13)] *Argelander-Institut für Astronomie, University of Bonn, auf dem Hügel 71, D-53121 Bonn, Germany.*

ABSTRACT

We compare various star formation rate (SFR) indicators for star-forming galaxies at $1.4 < z < 2.5$ in the COSMOS field. The main focus is on the SFRs from the far-IR (PACS-*Herschel* data) with those from the ultraviolet, for galaxies selected according to the BzK criterion. FIR-selected samples lead to a vastly different slope of the SFR-stellar mass (M_*) relation, compared to that of the dominant *main sequence* population as measured from the UV, since the FIR selection picks predominantly only a minority of *outliers*. However, there is overall agreement between the main sequences derived with the two SFR indicators, when stacking on the PACS maps the BzK-selected galaxies. The resulting logarithmic slope of the SFR-M_* relation is $\sim 0.8 - 0.9$, in agreement with that derived from the dust-corrected UV-luminosity. Exploiting deeper 24μm-*Spitzer* data we have characterized a sub-sample of galaxies with reddening and SFRs poorly constrained, as they are very faint in the B band. The combination of Herschel with Spitzer data have allowed us to largely break the age/reddening degeneracy for these intriguing sources, by distinguishing whether a galaxy is very red in B-z because of being heavily dust reddened, or whether because star formation has been (or is being) quenched. Finally, we have compared our SFR(UV) to the SFRs derived by stacking the radio data and to those derived from the Hα luminosity of a sample of star-forming galaxies at $1.4 < z < 1.7$. The two sets of SFRs are broadly consistent as they are with the SFRs derived from the UV and by stacking the corresponding PACS data in various mass bins.

Key words: cosmology: observations – galaxies: active – galaxies: evolution – galaxies: starburst – infrared: galaxies.

1 INTRODUCTION

Most galaxies at high redshifts are very actively forming stars, with star formation rates (SFR) of order of hun-

⋆ E-mail: giulia.rodighiero@unipd.it

dreds $M_\odot$ yr^{-1} being quite common. In the local Universe, instead, galaxies with such high SFRs are very rare and are called "ultraluminous infrared galaxies" (ULIRG, with $L_{\rm IR} > 10^{12}\,L_\odot$, Sanders et al. 1988). Such objects are caught in a transient, *starburst* event, likely driven by a merger having boosted both their SFR and their far-IR luminosity. By analogy, also such high-redshift galaxies were first regarded as starburst objects, until it became apparent that data were suggesting a radically different picture.

A first suspicion that a new paradigm was needed came from the discovery that over 80% of a "BzK" K-band selected sample of $z \sim 2$ galaxies were actually qualifying as ULIRGs (Daddi et al. 2005). Clearly, it was very unlikely that the vast majority of galaxies had all been caught in the middle of a transient event. As later shown, at high redshifts sustained SFRs ought to be the norm rather than the exception.

This was indeed demonstrated in a series of seminal papers (Elbaz et al. 2007; Daddi et al. 2007, Noeske et al. 2007), showing the existence of a tight correlation between SFR and stellar mass M_*, with

$$SFR \propto f(t) M_*^{1+\beta}, \quad (1)$$

which is followed by the majority of star-forming (SF) galaxies, with a dispersion of $\sim$ 0.3 dex, both at high redshifts (references above) and in the local Universe (Brinchmann et al. 2004). Thus, following Noeske et al. (2007) the correlation is called the *Main Sequence* (MS) of SF galaxies. Here $f(t)$ is a declining function of cosmic time (an increasing function of redshift). Furthermore, no signs of mergers have been found through dynamical measurements in many high redshift star forming galaxies (e.g. Förster Schreiber et al. 2009, Cresci et al. 2009, Law et al. 2009). Implying that most SF galaxies are in a quasi-steady SF regime, the existence of the MS has several important ramifications. It dictates a very rapid stellar mass growth of galaxies at early times, paralleled by a secular growth of their SFR itself (e.g., Renzini 2009; Peng et al. 2010), quite at odds with the widespread assumption of exponentially decling SFRs (as argued by e.g., Maraston et al. 2010 and Reddy et al. 2012). Even more importantly, the slope β controls the *relative* growth of high mass vs. low-mass galaxies, thus directly impinging on the evolution of the galaxy stellar mass function (Peng et al. 2013, see also Lilly et al. 2013).

While the existence of the MS is generally undisputed, its slope and width may differ significantly from one observational study to another, depending on the sample selection and the adopted SFR and stellar mass diagnostics. Selecting galaxies in a passband that is directly sensitive to the SFR (such as the rest-frame UV or the far IR) automatically induces a Malmquist bias in favor of low-mass galaxies with above average SFRs, thus flattening the resulting SFR$-M_*$ relation. This effect is clearly seen in Herschel FIR-selected samples, where formally $\beta \simeq -1$, but where only a tiny fraction of galaxies are detected at low stellar masses, i.e., those few really starbursting ones (Rodighiero et al. 2010a, 2011). This Malmquist bias has also been recognized in simulations (Reddy et al. 2012).

If redshifts are measured spectroscopically, the final sample may still suffer a similar bias even if the original photometric selection ensured a mass-limited input catalog. Indeed, at low masses the success rate of getting redshifts may be higher if the SFR is above average, and it may be lower at high masses if such galaxies are heavily extincted. Again, both these effects will tend to flatten the SFR$-M_*$ relation.

For example, Reddy et al. (2006) and Erb et al. (2006) found no positive correlation at all between SFR and stellar mass (i.e., $\beta \sim -1$) for a spectroscopic sample of UV-selected galaxies at $z \sim 2$, whereas Reddy et al. (2012) found an almost perfectly linear relation ($\beta \sim 0$) for a sample of similarly selected galaxies, when taking into account the result of their simulation.

On the other hand, other biases may tend to steepen the derived SFR$-M_*$ relation. Indeed, the mere selection of SF galaxies (e.g., by color or by a SFR cut) may preferentially exclude massive galaxies with below-average SFR.

At low redshifts the most suitable SFR indicator is the Hα luminosity (see Domínguez Sánchez et al. 2012), which is available for the extremely large sample of SDSS galaxies for which Brinchmann et al. (2004) and Peng et al. (2010) got $\beta \simeq -0.1$ using this SFR indicator. However, already at relatively low redshift Hα moves out of the optical range and Noeske et al. (2007) resorted on the 24 μm flux together with the less reliable [OII] luminosity as SFR indicators, deriving $\beta \simeq -0.3$ for their sample of $0.2 < z < 0.7$ galaxies. Conversely, Elbaz et al. (2007) got $\beta \simeq -0.1$ for star-forming galaxies at $z \sim 1$ using the Mid-IR (24 μm flux) as a SFR indicator. The same $\beta \simeq -0.1$ slope was then found by Daddi et al. (2007) for a mass-selected sample of $z \sim 2$ galaxies, using the extinction-corrected UV luminosity to measure SFRs. Finally, by combining 24 μm detection and SED fitting, Santini et al. (2009) found a similar value of $\beta \simeq -0.15$ for star-forming galaxies at $z \simeq 2$.

Stacking 1.4 GHz radio data in various mass bins proved to be another effective way of measuring the slope (and normalization) of the SFR$-M_*$ relation, with Pannella et al. (2009) getting $\beta \simeq 0$ for galaxies at $z \sim 2$. However, stacking the same radio data Karim et al. (2011) found $\beta \simeq -0.4$ for their sample of SF galaxies, having defined them as those bluer than $(NUV - r^+)_{\rm rest} = 3.5$, a definition that following Ilbert et al. (2010) includes both "active" ($(NUV - r^+)_{\rm rest} < 1.2$) and "intermediate" ($1.2 < (NUV - r^+)_{\rm rest} < 3.5$) SF galaxies. Restricting to "active" galaxies, Karim et al. found β oscillating between ~ 0 and ~ -0.2 with no obvious trend with redshift.

In summary, these examples illustrate that the derived value of the slope β critically depends on several assumptions and adopted procedures, namely:

- The starting photometric selection. For example magnitude/flux limited, (multi-)color selection or mass limited.
- The procedure to measure redshifts. Spectroscopic redshifts add to the photometric selection their instrument-specific selection function (i.e., the success rate as a function of photometric magnitudes and colors). Photometric redshifts are less biasing in this respect, modulo their occasional catastrophic failure.
- The criterion to separate SF from non-SF galaxies. As mass quenching dominates at high redshifts (Peng et al. 2010), a SF criterion that may retain galaxies on their way to be quenched would bias β towards more negative values.
- The adopted SFR indicator, including in it the procedure to estimate the dust extinction, if required.

• The explored mass range, as the slope at low masses might differ from that at high masses.

In this paper we derive the SFR$-M_*$ relation for a mass-complete sample of SF galaxies at $1.4 < z < 2.5$ using a variety of SFR indicators, such as the UV continuum, the Hα luminosity, the Mid-IR 24 μm flux, the FIR luminosity, and the radio luminosity, then stacking data when appropriate to derive the average SFR$-M_*$ relation for the mass-limited sample.

Throughout the paper we use a Salpeter (1955) initial mass function (IMF) and we assume $H_0 = 70$ km s^{-1}, $\Omega_\Lambda = 0.75$, $\Omega_M = 0.25$ and AB magnitudes.

2 OBSERVATIONS AND SAMPLE SELECTION

Homogeneous samples of sources would ideally be required to compare the results of different SFR estimators in a meaningful way. Unfortunately, this is normally quite difficult as the selection functions tend to bias samples from various surveys having different depths, spectral ranges and selection wavelength (see e.g., Wuyts et al. 2011). In this paper we combine far-IR-selected (i.e., SFR-selected) and near-IR-selected (as a proxy to M_*-selected) star-forming samples in the COSMOS field (Scoville et al. 2007), having both UV- and IR-based SFR determinations (both mid- and far-IR). A fraction of them have been spectroscopically observed to measure the Hα emission line luminosity, providing an additional indicator of SFR. Radio observations from the literature are used to extend the comparison of widely used SFR tracers. We first describe the datasets used, the sample selections and the SFR and M_* measurements.

We consider only galaxies within the redshift range of $1.4 \lesssim z \lesssim 2.5$, based either on spectroscopic or photometric redshifts.

2.1 Herschel far-IR samples

We start from the sample of PACS/*Herschel* observations in the COSMOS field described by Rodighiero et al. (2011), over 2.04 square degrees and down to a 5σ detection, above confusion limits of 8 and 17 mJy at 100 and 160 μm, respectively (Lutz et al. 2011). Photometry was carried out by PSF-fitting at 24μm prior positions. The detection limits correspond to $\sim 100\,M_\odot$ yr^{-1}, $\sim 200\,M_\odot$ yr^{-1} and $\sim 300\,M_\odot$ yr^{-1}, respectively at $z = 1.5$, 2 and 2.5. Over a common area of 1.73 square degrees we cross-matched the PACS detections with the IRAC-selected catalog of Ilbert et al. (2010), so to obtain UV-to-8μm photometry, accurate photometric redshifts and stellar masses by SED fits as described in Rodighiero et al. (2010b). At $z \sim 2$ the sample of Ilbert et al. (2010) is complete in mass above $\sim 10^{10} M_\odot$ for star-forming galaxies (see their Table 3). FIR $8 - 1,000\,\mu$m luminosities ($L_{\rm IR}$) are derived from PACS fluxes using a set of empirical templates as described in Rodighiero et al. (2010b) and Rodighiero et al. (2011). In this work IR luminosities are always converted to SFR as SFR$[M_\odot {\rm yr}^{-1}] = 1.7 \times 10^{-10} L_{\rm IR}[L_\odot]$ (Kennicutt 1998, hereafter SFR(FIR)). By adopting different templates or codes, consistent SFR estimates are obtained with no bias and a scatter of ~ 0.15 dex (that represents the typical error associated to our SFRs, see also Berta et al. 2013). The dataset includes in total 576 PACS-detected galaxies with $1.4 < z_{\rm phot} < 2.5$.

2.2 BzK samples

We use the K-band selected sample of $1.4 < z < 2.5$ star-forming galaxies down to $K_{\rm s,AB} < 23$ in the COSMOS field (McCracken et al. 2010) selected according to the criterion (Daddi et al. 2004) designed to pick star-forming galaxies at these redshifts (the so-called star-forming BzK, or sBzK), i.e., those sources with:

$$(z - K)_{\rm AB} - (B - z)_{\rm AB} \geqslant -0.2. \quad (2)$$

The passively evolving BzK (or pBzK) are not discussed in this paper, apart from the possible contamination of the formal sBzK sample. Stellar masses have been computed following the same procedure as in Daddi et al. (2004) and Daddi et al. (2007), adopting the empirically calibrated relation based on the BzK photometry alone:

$$\log(M_*) = -0.4(K_{\rm tot} - 19.51) + 0.218(z - K) - 0.499. \quad (3)$$

In spite of its simplicity, the procedure gives stellar masses which with a 0.3 dex scatter are in excellent agreement with those obtained with full fledged SED fits. For all selected sBzK the SFRs are estimated from the UV rest-frame luminosity corrected for dust extinction (hereafter SFR(UV)), with reddening being inferred from the slope of the UV continuum as in Daddi et al. (2007). UV-based SFRs reach down to few $M_\odot$ yr^{-1} at $z \sim 2$. The final sBzK sample includes a total of 25,574 sources in the redshift range $1.4 < z < 2.5$. For the rest of the paper we will use consistently these stellar masses unless stated otherwise. In Rodighiero et al. (2011) we verified that they are fully consistent with those used in Rodighiero et al. (2010b) and in the previous subsection.

• *good*-sBzK: with a formal error $\delta\log[{\rm SFR(UV)}] < 0.3$ dex (21,375 sources);

• *bad*-sBzK: with a formal error $\delta\log[{\rm SFR(UV)}] > 0.3$ dex (4,199 sources).

The relative uncertainty on SFR(UV) is formally derived by propagating the errors on the optical photometry of each source, in particular from the B and z bands used to compute $E(B-V)$ and then to derive a dust-corrected SFR(UV) (see Daddi et al. 2004):

$$\delta\log[SFR(UV)] = \sqrt{E1^2 + E2^2 + E3^2 + E4^2}, \quad (4)$$

with $E1 = 0.6 \times \delta B$, $E2 = \delta z$, $E3 = 0.1$ and $E4 = (0.75 \times 0.06 \times (1 + z_{\rm phot}))$, where δB and δz are the photometric errors on the B and z magnitudes and 0.1 is a term that accounts for the error on the estimate of the total magnitude of the galaxy. Note that the different coefficients of δB and δz stem from the B magnitude entering twice in the calculation of the SFR, once to estimate the reddening and once to measure the observed UV luminosity, whereas the z magnitude affects only the reddening estimate. The last term ($E4$) accounts for the uncertainty of the photometric redshift where we assume the typical $\delta z_{\rm phot}/(1 + z_{\rm phot}) \sim 0.06$ and 0.75 is an empirical coefficient depending on the typical UV slope and luminosity distance of the objects.

The *good*-sBzK sample selection represents ∼84% of the whole sBzK population, and can be considered as a criterium

to select reliable SFR(UV) estimates (at least at the limits of the COSMOS survey).

We should mention that among the ∼16% of the *bad*-sBzK sources, ∼5% of them are undetected in the B band (at the COSMOS survey depth), implying that their SFR(UV) can not simply be computed or classified. These sources will be considered in the *Herschel* stacking analysis and will be still included in the *bad*-sBzk classification. However, when showing the SFR(UV) for the single sources in the *bad*- and *good*-sBzK sample, they will not be reported.

In principle, the BzK criterion may introduce a bias by selecting only part of the star-forming galaxies in the explored redshift range. The same would also do a pure photometric redshift selection, given the sizable number of photometric redshifts which are grossly discrepant with respect to spectroscopic redshifts (especially at $1.4 < z < 1.8$, cf. Ilbert et al. 2010). For this reason we have inspected the Ilbert et al. catalog, finding that $\sim 6\%$ of $1.4 < z_{\rm phot} < 2.5$, $M_* > 10^{10}$ M$_\odot$ objects are missed by the BzK criterion (including both star-forming and passive sources). However, a major fraction of them lie very close to the line defined by Equation (2), hence just small photometric errors have driven them out of the sBzK domain. The others are likely cases in which $z_{\rm phot}$ fails catastrophically. Thus, we believe that a sample of sBzK-selected galaxies with $1.4 < z_{\rm phot} < 2.5$ is more robust than either a purely sBzK- or a purely $< z_{\rm phot}$-selected sample. In any case, slope and dispersion of the SFR(UV)$-M_*$ main sequence are not appreciably affected by the inclusion of this minority population.

2.3 Hα spectroscopic sample

As part of a Subaru telescope survey with FMOS (Fiber Multi-Object Spectrograph) in its high-resolution mode ($R \sim 2600$), the sBzK population in the inner deg^2 of the COSMOS field has been targeted to detect $H\alpha$ in emission from galaxies at $1.4 \lesssim z \lesssim 1.7$ (Kashino et al. 2013; Zahid et al. 2013, Silverman et al. in prep.). Sources have been selected from the sample described in Section 2.2 to have stellar masses $> 10^{10} M_\odot$ and to belong to the *good*-sBzK population.

The measured Hα luminosities for the 162 best quality (flag=2) detections are converted to SFR (hereafter SFR(Hα)) with the Kennicutt (1998) relation, SFR(Hα)$[M_\odot {\rm yr}^{-1}] = 3.03 \times 10^{-8} L({\rm H}\alpha)/L_\odot$. The H$\alpha$ luminosity has been corrected for extinction applying the average $A_{H\alpha} - M_*$ relation from the Balmer decrement of FMOS spectra stacked in mass bins (Kashino et al. 2013).

3 SFR FROM VARIOUS INDICATORS

In this section we present a systematic comparison of SFRs from various widely used SFR indicators, focusing in particular on their effect on the SFR-stellar mass relation of our program galaxies at $1.4 < z < 2.5$.

3.1 Far-Infrared versus Ultraviolet SFRs

Figure 1 (left panel) compares the SFRs from the far-IR and from the ultraviolet, i.e., SFR(FIR) vs. SFR(UV). We used the sample of 473 sBzK at $1.4 < z < 2.5$ in the COSMOS field for which a PACS counterpart is available. It is apparent that the calorimetric indicator, able to almost completely reveal the hidden SFR, provides systematically higher values than SFR(UV), in particular at SFR(UV)$\lesssim$300 $M_\odot$ yr^{-1}[1]. This is commonly interpreted as an underestimate of dust extinction as derived from the UV slope (i.e., from the $B - z$ color, as in Daddi et al. 2007, having potentially an important impact on the slope and scatter of the star-forming main sequence. This is shown in the right panel of Figure 1, where we show the mass-SFR relation for the parent sample of *good*-sBzK (small black dots). To emphasize the effect of different SFR indicators in shaping the MS, for the PACS sources shown in the left panel, the right panel displays both their SFR(FIR) (red filled circles) and their SFR(UV) (green open circles), while using the same stellar mass. By relying only on SFR(FIR), one gets a flat SFR$-M_*$ relation, with $\beta \simeq -1$ in Equation (1). Such a flat relation is the direct result of having selected galaxies using a far-IR flux limited sample, which translates indeed into a SFR-limited sample. On the other hand, the UV indicator provides a much steeper relation (solid line in Figure 1, with $\beta = -0.21$, *good*-sBzK only, Rodighiero et al. 2011). This illustrates the point made in the Introduction, about how different the slope of the MS can result when using different selection criteria or SFR indicators.

This apparent discrepancy derives from the vastly different number of galaxies recovered by the two selections, the Herschel/SFR-selected sample and the sBzK/mass-selected sample. As made clear in Figure 1 (right panel), for $\log(M_*) \lesssim 11$ only a few sBzK galaxies are individually detected by Herschel, and include (part of) the $\sim 2\%$ *outliers* from the MS as shown by Rodighiero et al. (2011). We interpreted these objects as obscured starbursts, possibly driven by merging events or major disk instabilities, characterized by high specific-SFR (sSFR=SFR/M_*), and where $E(B-V)$ and the SFR from the UV are systematically underestimated.

On the other hand, the Herschel-COSMOS data at these redshifts do not reach below SFR $\sim 200 M_\odot$ yr^{-1} and therefore to recover a far-IR MS we must resort on stacking the Herschel data at the location of sBzK-selected galaxies, which represent a mass-selected sample. To this end, we split the sBzK sample into four mass bins, and stack all PACS-undetected sBzK if a residual 160μm map created by removing all PACS 160μm detections with SNR$>$ 3 (stacking at 100μm does nwellot change our results). The stacking is performed using the IAS stacking library (Béthermin et al. 2010), PSF-fitting photometry, and applying an appropriate flux correction for faint, non-masked sources to the PACS stacks (Popesso et al. 2012). With this procedure, we derived the average flux for each mass bin. Using the formalism introduced by Magnelli et al. (2009), that accounts both for detections and no-detections, we then converted these stacked fluxes into bolometric luminosities $L_{\rm IR}$ by adopting an average K-correction (Chary & Elbaz 2001) and then into SFR through the standard law of Kennicutt (1998). bog

[1] This can be the case if the detected rest frame UV is emitted from a relatively unobscured region of the galaxy, whereas most of the SF activity is heavily extincted.

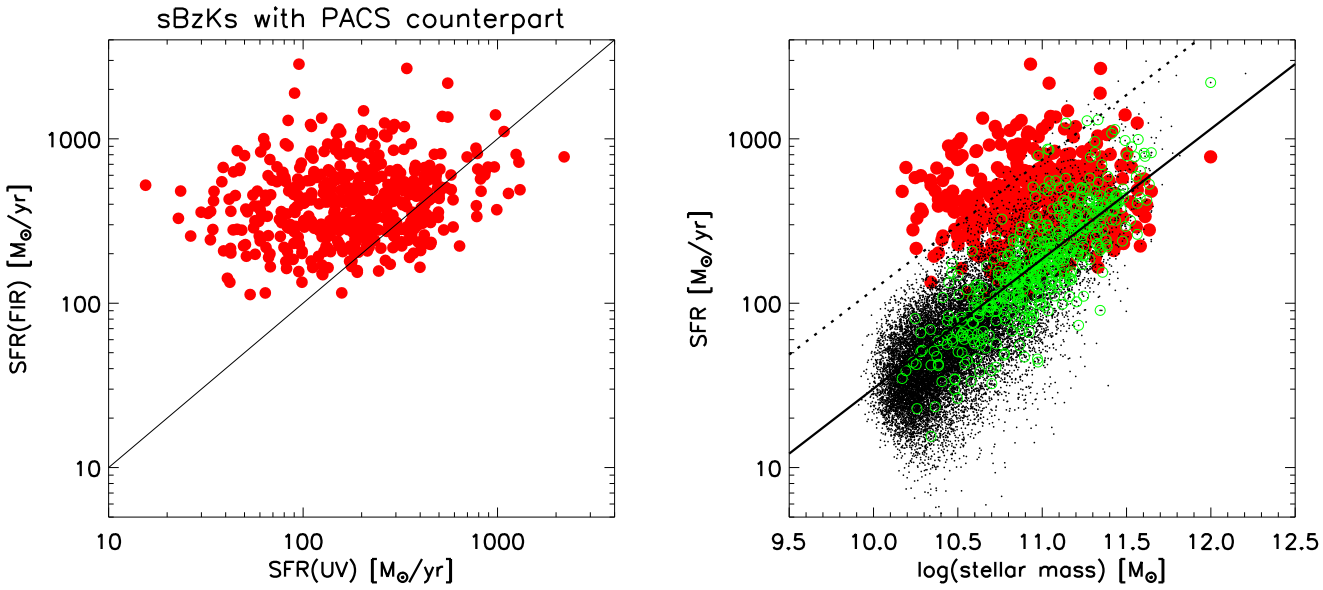

Figure 1. *Left panel*: comparison of SFR(UV) and SFR(FIR) for a sample of 473 sBzK at $1.4 < z < 2.5$ with a PACS/*Herschel* detection in the COSMOS field. The *right panel* shows the SFR-stellar mass relation for various samples, namely: parent sBzK sample (the so-called *good* subsample, see text for details, small black dots) for which SFR(UV) is reported, the PACS-detected sBzK sources shown in the upper panel, with SFR(FIR), and for the same group of galaxies the green open circles represent the corresponding SFR(UV). The solid (dotted) line indicates the MS (SFR(UV)= 4×SFR(MS)) relation at $z \sim 2$ (Rodighiero et al. 2011).

The results of this procedure are presented in Figure 2. We considered the whole sBzK sample at $1.4 < z < 2.5$, and then separately the *good*- and *bad*-sBzK sub-samples, represented by small black dots and small magenta dots, respectively. The big red filled circles show the average SFR derived by stacking on the PACS maps only the *good*-sBzK (with the corresponding best linear fit shown as a dashed red line, slope $\alpha = 1 - \beta = 0.86 \pm 0.08$). The magenta circles refer instead to the stacking results for the *bad*-sBzK (slope $\alpha = 1 - \beta = 0.47 \pm 0.12$) whereas the green data points represent the SFR obtained by stacking the whole sBzK population, with the corresponding best linear fit shown as a dashed green line (slope $\alpha = 1 - \beta = 0.74 \pm 0.11$).

Overall, there is a nice agreement of SFR(UV) and stacked SFR(FIR) for the *good*-sBzK sample, largely amending the discrepant results when using only the individually PACS-detected sources (Figure 1). The MS slope using SFR(FIR) ($\alpha = 1 - \beta = 0.86 \pm 0.11$) is consistent within the errors with that derived using SFR(UV) (α=1 − β=0.79±0.10, Rodighiero et al. 2011). This argues for the correlation of SFR(UV) and SFR(FIR) to be fairly good for the general MS population at $z \sim 2$, a correlation that instead clearly fails catastrophically for the most obscured starburst sources, which represent only few percent of the star-forming galaxies at the same cosmic epoch (Figure 1). Still, it is somewhat intriguing that for these galaxies (the green open circles in Figure 1) the 'wrong' SFR(UV) places them within the main sequence, probably because the optical colours refer only the small fraction of the SFR which is not fully buried in dust.

Figure 3 further illustrates and quantifies these findings. The data points represent the SFR(FIR)/SFR(UV) ratio for the *good*-sBzK galaxies which are individually detected by the Herschel/PACS PEP survey over the COSMOS field. At low masses this ratio is very high (~ 10) and decreases with increasing mass reaching near unity towards the high mass end. However, at low masses only 0.4% of the *good*-sBzK galaxies are detected in the infrared, i.e., only the extreme outliers. Then the fraction of FIR-detected galaxies increases with stellar mass, reaching $\sim$ 16% at the top end. This is still far from 100%, as the PEP data are not deep enough to recover all galaxies even at the top mass end. Notice that the minimum measured SFR(FIR) ($\simeq 200\, M_{\odot} \mathrm{yr}^{-1}$) refers to $z = 2$, and increases with redshifts, whereas the completeness of the PEP catalog starts dropping at substantially higher values (Rodighiero et al. 2011). In deeper PEP observations, such as those on the GOODS-South field, the fraction of massive galaxies which are detected does indeed approach 100% (Rodighiero et al. 2011). A further confirmation that SFR(UV) does not systematically deviate from SFR(FIR) comes from the stacking of the Herschel/PACS data discussed above and illustrated in Figure 2. The almost horizontal line in Figure 3 shows the ratio of the best fit SFR(FIR)$-M_*$ and SFR(UV)$-M_*$ relations from Figure 2, thus emphasizing that both methods of deriving the SFR are fully consistent for the vast majority of the galaxies, with the exception of a lesser minority of outliers.

When including all sBzK in the far-IR comparison (green circles and green line), the slope of the *Herschel* derived MS ($\alpha = 1 - \beta = 0.74 \pm 0.08$) is still largely overlapping with that derived from the UV. For what concerns the *bad*-sBzK sample alone, Figure 2 indicates that at low masses ($M_* < 10^{11} M_{\odot}$) the mean SFR(FIR) is consistent with that of the most reliable SFR(UV) sample, while at higher masses it is systematically lower, hinting for a contamination by passive sources into the star-forming color selection. To check for this possibility in the next section we

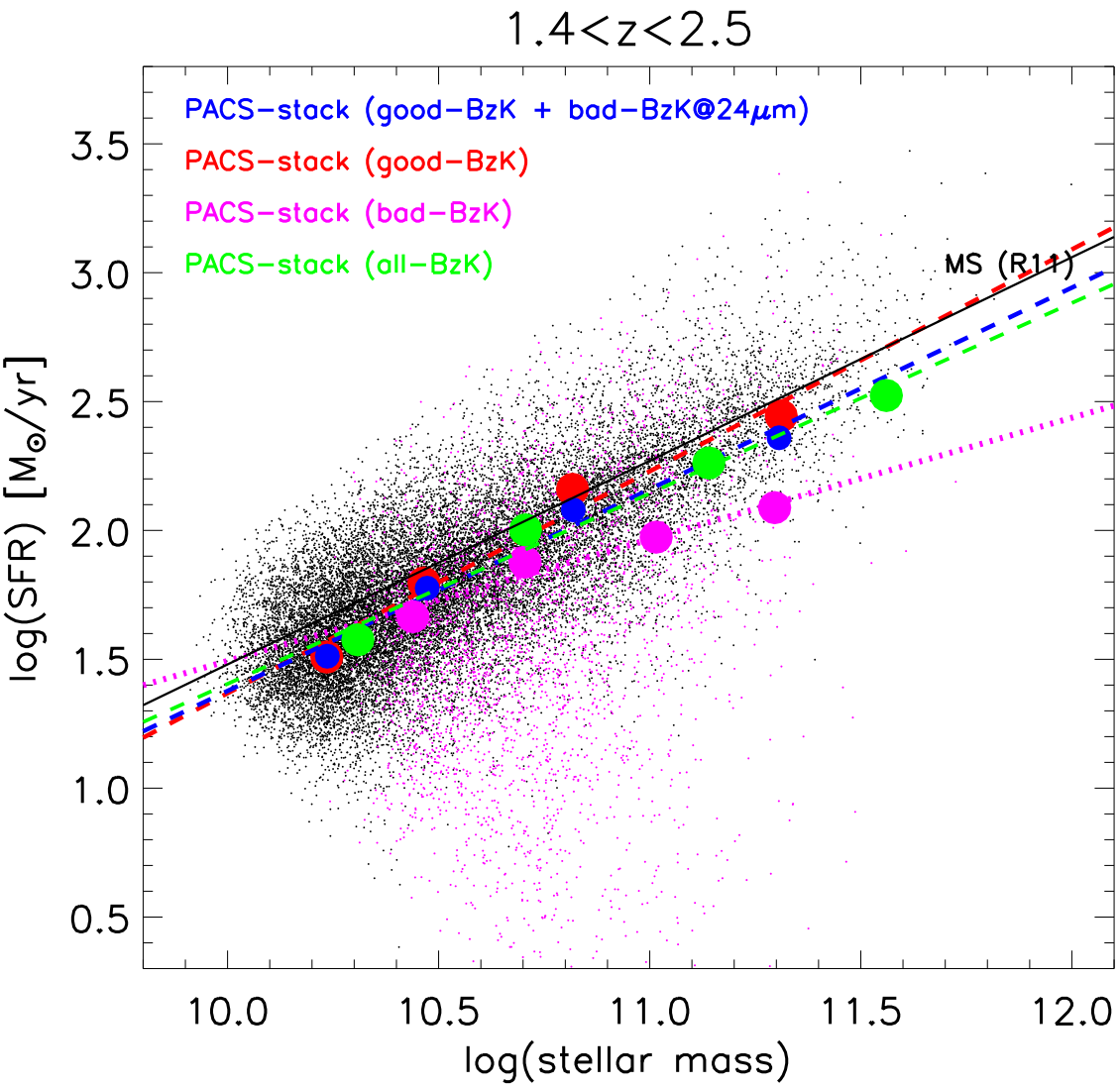

Figure 2. The SFR-stellar mass relation for star-forming galaxies at $1.4 < z < 2.5$ is shown for various samples: the small black dots represent the parent *good*-sBzK. Most of these sources have a reliable estimate of extinction from the $(B - z)$ color, and thus a reliable SFR from the UV. The complementary sample of sBzK for which SFR(UV) is much less reliable (*bad*-sBzK), is shown with small magenta dots. These sBzK samples have been split into four mass bins. The red filled circles show the average SFR derived by stacking on the PACS maps the *good*-sBzK (with the corresponding best linear fit shown as a dashed red line), while the magenta circles refer to the stacking results for the *bad*-sBzK (with the corresponding best linear fit shown as a dashed magenta line). Green filled circles represent the SFR obtained by stacking the whole sBzK population in the four different mass bins (with the corresponding best linear fit shown as a dashed green line). The blue circles correspond to the stack of the *good*-sBzK sample plus the *bad*-sBzK which are detected at 24 μm, and the corresponding best fit is shown as the blue dashed line. For each mass bin the error bars on SFR are derived from the bootstrap statistical stacking analysis and are smaller than the symbol sizes. The solid black line represents the best fit to the Main Sequence derived by Rodighiero et al. (2011).

consider the MIPS 24μm properties of these galaxies and we further expand on this issue.

3.2 Mid-Infrared versus Ultraviolet SFRs

A natural extension of the *Herschel* based SFR analysis includes the widely used 24 μm MIPS/*Spitzer* flux density, that allows one to reach lower SFRs than *Herschel*, although with the large extrapolation required to estimate the total IR luminosity (e.g. Elbaz et al. 2007, Elbaz et al. 2011, Wuyts et al. 2011). Since the earlier *Herschel* investigations it was realized that the 24 μm SFR indicator was working very well up to redshift ~ 1, while it starts to fails at higher redshifts by overestimating somewhat the true $L_{\rm IR}$ (Nordon et al. 2010, Nordon et al. 2012, Rodighiero et al. 2010b, Elbaz et al. 2011). This is particularly critical at $z \sim 2$, where the PAH features enter the observed 24 μm pass-band. More recently, Magdis et al. (2012) have undertaken a systematic study of the typical SED of normal star-forming and starburst galaxies at $z \sim 2$, including both

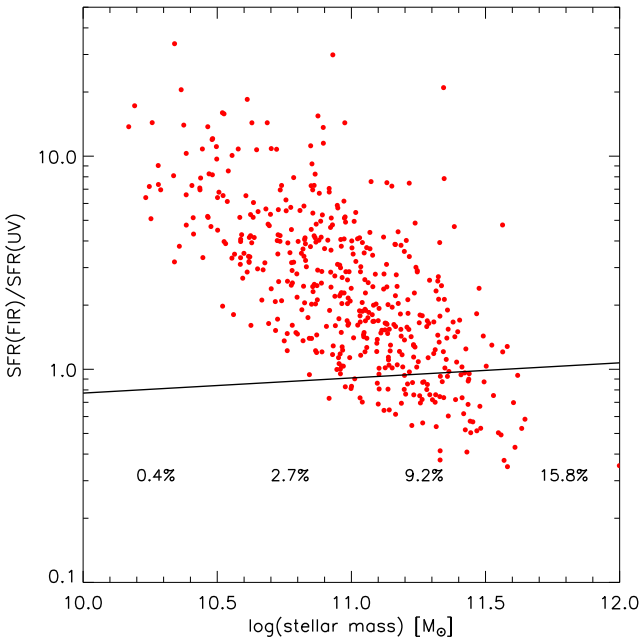

Figure 3. The SFR(FIR)/SFR(UV) ratio for galaxies that are individually detected by Herschel/PACS over the COSMOS field (red points). The fractions of such detected sources over the parent *good*-sBzK population are given for four mass bins, each 0.5 dex wide. The nearly horizontal line represents the ratio of the best fit SFR(FIR)$-M_*$ and SFR(UV)$-M_*$ relations from Figure 2.

PACS and SPIRE/*Herschel* data in their analysis. They found that the mean SED does not evolve along the MS at $z \sim 2$, while it differs for the starburst population (characterized by a warmer dust component). Similar results are found also by Elbaz et al. (2011). These new investigations revamped the use of the 24 μm SFR indicator, ideally allowing the adoption of a universal SED to extrapolate $L_{\rm IR}$ for MS sources. Other recipes and methods have been presented to recalibrate the 24 μm flux density (Nordon et al. 2012; Wuyts et al. 2011; see also Berta et al. 2013 for a summary). In this Section we adopt the MS templates of Magdis et al. (2012) to extrapolate $L_{\rm IR}$ from the 24 μm flux densities.

Following the same approach of Section 3.1, in Figure 4 (left panels) we compare SFR(UV) with SFR($24_{\mu\rm m}$) for the sample of sBzK in COSMOS with a 24 μm counterpart brighter than $S_{24\mu\rm m} > 60\mu$Jy. The corresponding differences induced in the MS relation are instead shown in the right-hand panels. We separate the analysis including all sBzK (top panels) and only the *good*-sBzK (bottom panels). Red points represent the sBzK/MIPS-detected sources shown in the left panels, with SFR from $L_{\rm IR}$ extrapolated from the 24μm flux density. The green points are the same sources plotted with the corresponding SFR(UV). For completeness, we report also SFR(UV) for the parent sBzK sample (small black dots). The solid (dotted) line indicates the MS ($\times$4MS) relation at $z \sim 2$ (Rodighiero et al. 2011), as in Figure 1. The considered flux limit allows us to reach SFR as low as $\sim 60 M_\odot$ yr^{-1}, diving well into the MS, but it still shows the almost flat SFR$-M_*$ relation which is typical of SFR-selected samples (see Figure 4, right panels).

This SFR(UV)-SFR($24_{\mu\rm m}$) relation including all sBzK sources is rather dispersed, showing, as for the SFR(UV)-SFR(IR), an excess of objects with SFR($24_{\mu\rm m}$) > SFR(UV), particularly for SFR(UV)$<$ 100 $M_\odot$ yr^{-1}. Indeed, the penalty of a wrong (underestimated) extinction correction is evident for the sBzK sources with a less reliable SFR(UV) (the *bad*-sBzK): in the top-left panel the tail at low SFR(UV) ($\lesssim 10\, M_\odot$ yr^{-1}) is populated by these objects, that instead largely disappear when considering only the *good*-sBzK (bottom-left panel). In this case the MS based on SFR($24_{\mu\rm m}$) nicely overlaps with the UV-based one, with the advantage of unraveling also the starburst sources (with SFR$>$ 4$\times$SFR(MS)) that remain unidentified when using SFR(UV). Thus, the mid-IR reveals this population of main sequence *outliers*, as does the far-IR (Rodighiero et al. 2011), but the extrapolation required to derive $L_{\rm IR}$ from the 24 μm flux density still makes the far-IR information a more direct and effective mean to estimate the global SFR of high-redshift dusty sources.

The *bad*-sBzK which are detected at 24 μm are clearly star forming and therefore should be considered together with the *good*-sBzK when stacking the *Hershel* data to derive the slope and zero point of the main sequence. The result is illustrated in Figure 2 (blue circles and dashed line) and the corresponding slope is $\alpha = 1 - \beta = 0.80 \pm 0.07$. We consider this as our best possible estimate of the main sequence slope at $z \sim 2$.

The 24 μm flux density allows us also to better characterize the population of the *bad*-sBzK. For example, among the 3219 sBzK galaxies with $M_* > 10^{11} M_\odot$ in our sample there are 787 such objects, $\sim$ 60% of which (467) are not detected at 24 μm, corresponding to a SFR upper limit of $\sim 60\, M_\odot$ yr^{-1}. This is well below the SFR of massive MS galaxies and we infer that most of the 467 *bad*-sBzK are likely to be well on their way to be quenched. This is further reinforced by the result of stacking the Herschel 160 μm data, separately for the 24 μm detected and undetected *bad*-sBzK, as displayed in Figure 5. Clearly, on average the 24 μm undetected *bad*-sBzK galaxies lie well below the MS, whereas the 24 μm detected ones lie appreciably below the MS and exhibit a shallower slope ($\alpha = 1 - \beta = 0.36 \pm 0.04$). We recall that our sBzK selection is supposed to pick star-forming galaxies, whereas now we have evidence that out of the original 25,574 sBzK $\sim$ 4199 of them ($\sim$ 16%) are likely to be quenched or on the way to be quenched. Of course, we cannot exclude that some of these galaxies are experiencing a temporary downward excursion from the main sequence and will return to it in the future, i.e., representing a tail of the main sequence itself. Data cannot distinguish between such objects and truly quenching ones. However, we note from Figure 6 that the bad-sBzK are confined to relatively high masses, where galaxies are faint in the B-band because they are either heavily reddened or because they are quenched or on the way to be quenched. In the former case they should be detected at 24 μm but they are not, which suggests they are actually quenched. Note also the absence of low mass bad-sBzK, while there should be many of them if they would represent a tail of the main sequence distribution. Moreover, Figure 5 shows that when stacking the FIR data for the 24 μm-undetected sources their average SFR

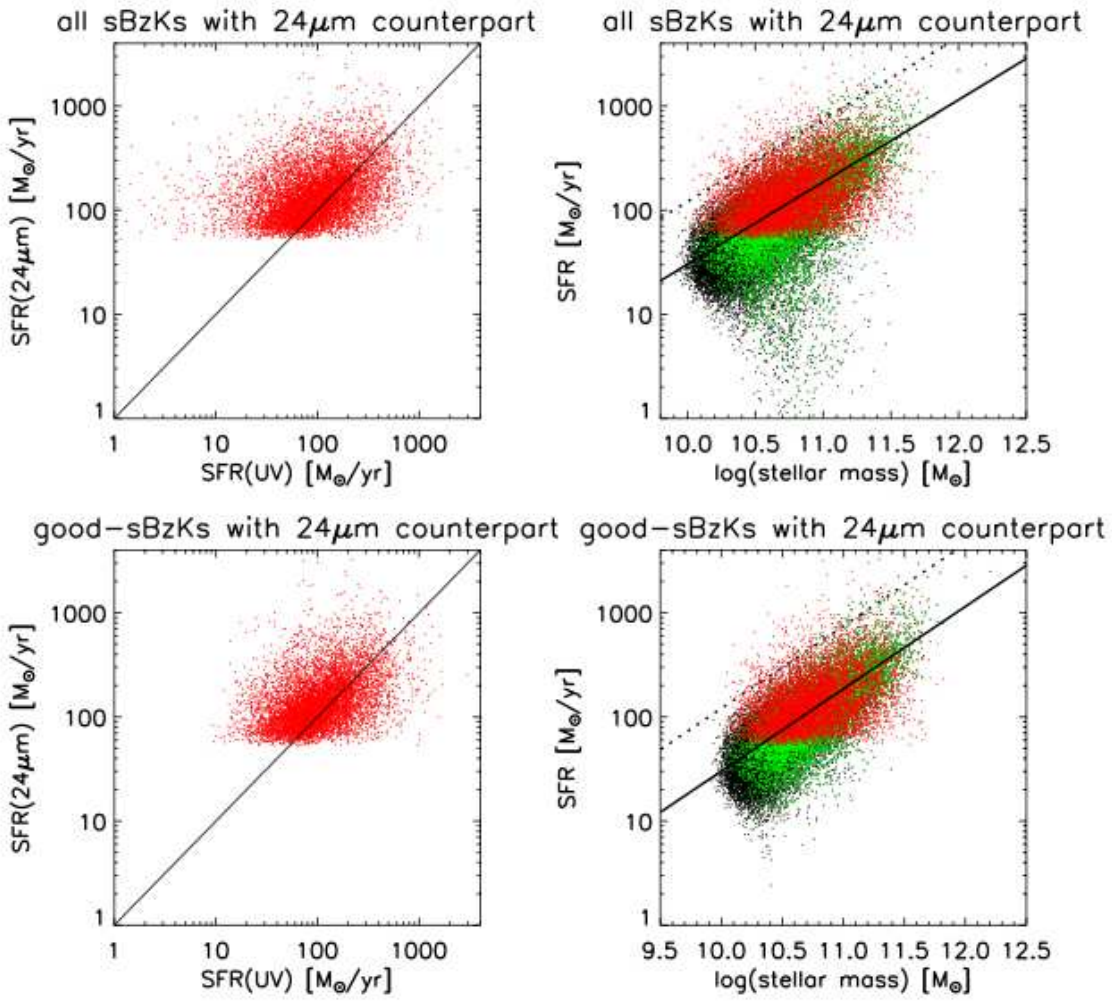

Figure 4. *Left panels*: comparison of SFR(UV) and SFR(24μm) for the sample of sBzK at $1.4 < z < 2.5$ with a MIPS/*Spitzer* 24μm detection ($S_{24\mu m} > 60\mu$Jy) in COSMOS. *Right panels*: the SFR-stellar mass relation of star forming galaxies as shaped by different SFR indicators: red points represent the sBzK/MIPS sources shown in the left panels. The green points are the same sources plotted with the corresponding SFR(UV). For completeness, we show also SFR(UV) for the parent sBzK sample (small black dots). The solid (dotted) line indicates the best fit to the Main Sequence as in Figure 1. *Upper panels* include all sBzK-selected galaxies, while *lower panels* report only the *good*-sBzK, for which a reliable estimate of the extinction is available from the UV slope.

is well below the main sequence values (from ~ 5 to ~ 30 times below) which suggests that the vast majority of them are likely to be quenched or on their way to be quenched. We believe this illustrates the capability of this multiwavelength approach of singling out MS galaxies as well as the starburst and quenched outliers on either side of the MS. *In summary, the bad-sBzKs include a mixture of actively star-forming galaxies and others which may be fully quenched or with SFRs well below the MS, though the distinclion between these two latter subclasses would need deeper data.*

3.3 BzK sources selected for being star-forming actually not being so

In our previous analysis we made an intensive use of the sBzK classification based on the relative error on SFR(UV) to understand the quality and limits of the SFR derived solely from the rest-frame UV. We have seen that, formally, when considering only reliable sources (i.e., ∼84% of the sBzK COSMOS sample, those with $\delta\log([\mathrm{SFR(UV)}])< 0.3$ dex) then SFR(UV) is in very good agreement with SFR(IR) for the vast majority of the galaxies. To better characterize the properties of these various sBzK classes, we present in Figure 6 the distribution of their stellar masses (top panel), SFR(UV) (second panel from top), B magnitudes (third panel from top) and redshifts (bottom panel). We report separately the distributions for the *good*-sBzK (dot-dashed red lines), the *bad*-sBzK (dashed blue lines), and the total distribution (solid black lines). Notice that the mass distribution starts dropping at $\sim 2\times10^{10}\,M_{\odot}$, which we consider the completeness limit of our sample. This is nearly twice as large as the mass limit of the Ilbert et al. (2010) $1.5 < z < 2$ sample, as our sample extends to $z = 2.5$.

As expected, the intrinsic larger errors on SFR(UV) (as propagated from formal errors on the original photometry) is mostly related to the faintness of these sources in

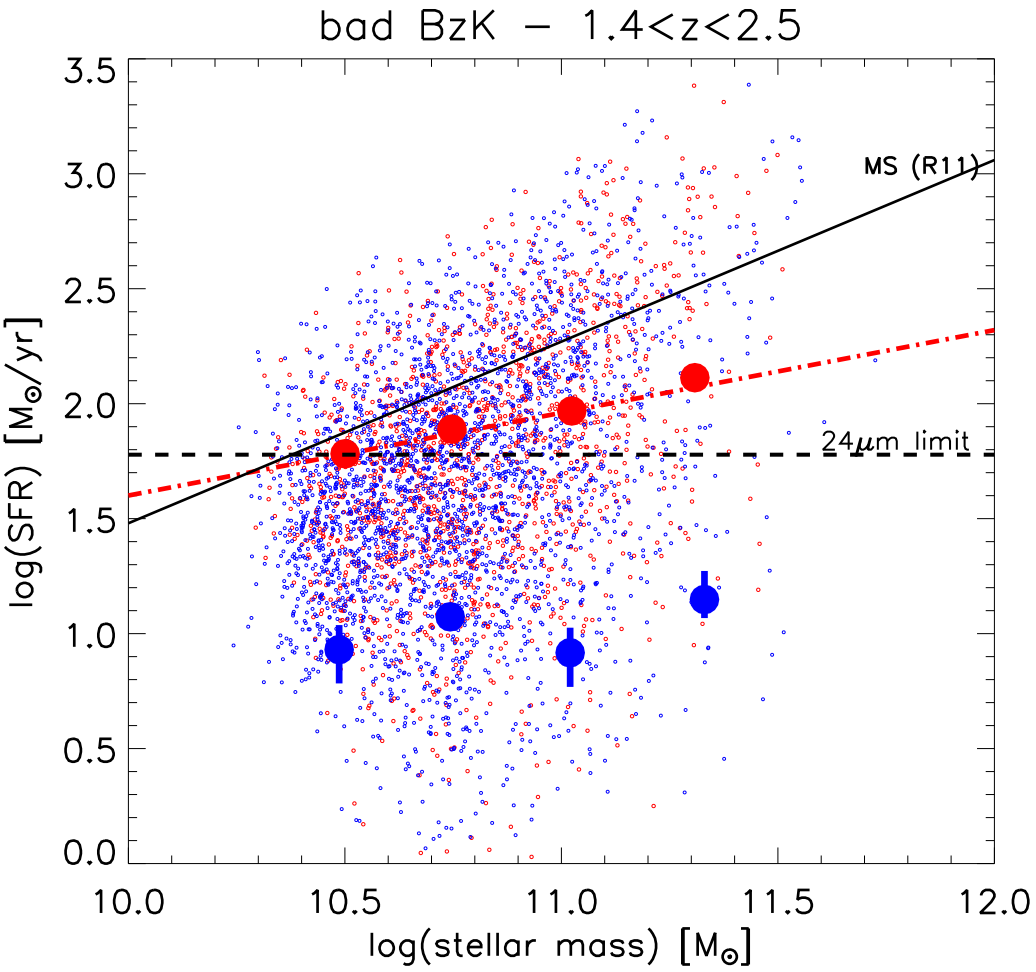

Figure 5. The SFR(UV)-stellar mass relation for the *bad*-sBzK with red symbols referring to the MIPS 24 μm detected sources and the blue symbols to the 24 μm undetected ones. The corresponding large circles show SFR(FIR) having stacked the *Herschel*/PACS data in four mass bins. The dashed horizontal line corresponds to the MIPS 24 μm sensitivity limit over the COSMOS field at $z = 2$ and the solid line is the same as in Figure 1. For each mass bin, error bars on SFR are derived from the bootstrap statistical stacking analysis and presented with the same color coding (if bigger than the symbol sizes).

the B band[2]: the peak of the observed B-band distribution is $\sim$2.5 mag brighter for the *good*-sBzK. On the contrary, the SFR(UV) distributions for the two samples span the same range, with the *bad* sources presenting only a tiny fraction excess at low SFR(UV), as already revealed in Figure 4. However, this low-SFR tail does not impact on the main trend for SFR(UV)-SFR(IR), as revealed by the PACS stacking analysis (Figure 2 and Section 3.1), and it consists of a mixture of two opposite kinds of sources: 1) passive sources that appear to fulfill the Equation 2 star-forming (sBzK) selection because of their large error in the B-band magnitude, and 2) very obscured/starburst objects for which SFR from the UV catastrophically fails (as it does for a small minority of the *good*-sBzK as well).

[2] The faintness of the bad-sBzK in the B band does not primarily derive from the relative distance of such class, since their redshift distribution is almost flat over the whole range (see Figure 6, bottom panel), although the ratio of bad- to good-sBzKs moderately increases with redshift.

In this respect, we can notice on Figure 5 that quite many of the most massive *bad*-sBzK exhibit a SFR(UV) well in excess of the MS values, whereas their average SFR(IR) from stacking the Herschel data falls well below the MS. We conclude that the population of the *bad*-sBzK is indeed a mixture of obscured starburst and of quenching galaxies, with the former ones dominating at lower masses and the latter ones dominating at high masses. This trend can be readily understood when considering that the fraction of (starburst) MS outliers ($\sim$ 2%) is fairly independent of stellar mass (Rodighiero et al. 2011), hence low mass outliers must be more numerous, whereas at high masses the *mass-quenching* mechanism of Peng et al. (2010) must be proceeding at full steam at these redshifts. We also notice that for the *bad*, 24 μm undetected sBzK the procedure to get the SFR from UV is delivering a SFR about an order of magnitude too high because it mistakes the red $B-z$ color as due to reddening, while it is due to old age. Thus, the *bad* fraction of the star-forming selection is effectively contaminated by a number of galaxies which are either already quenched

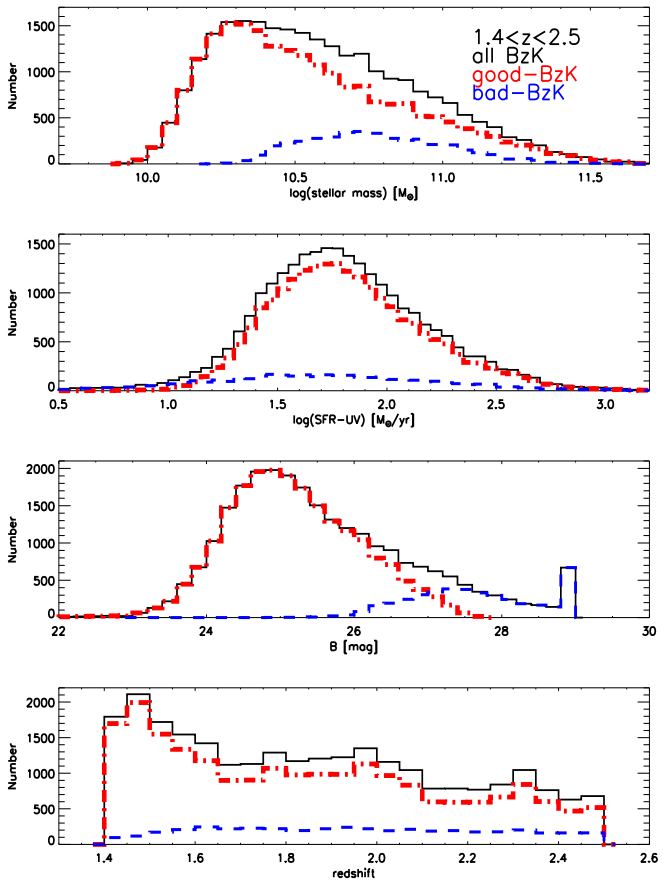

Figure 6. Statistics of the sBzK sample at $1.4 < z < 2.5$ in the COSMOS field, as a function of stellar mass (*top panel*), SFR(UV) (*second panel from top*), observed B magnitude (*second panel from top*) and redshift distributions (*bottom panel*). We report the distribution of sBzK sources with reliable SFR(UV) (i.e. *good*-sBzK, dot-dashed red lines), the *bad*-sBzK (dashed blue lines), and the total distribution (solid black lines). Objects undetected in the B band are all assigned to the faintest bin of the B-band histogram. The redshift distribution of the three populations is shown in the bottom panel.

or being quenched. These amount to $\sim 60\%$ of the *bad*-sBzK sample of galaxies more massive than $10^{11}\,M_{\odot}$, or $\sim 15\%$ of the whole sBzK sample above this mass limit. Ironically, for most *bad*-sBzK, many of those with very high SFR(UV) are actually quenched (the small blue point in Figure 5 with SFR(UV)$>>60\,M_{\odot}$ yr^{-1}) and many of those with very low SFR(UV) are actually starbursting (the small red points in the same figure with SFR(UV)$<<60\,M_{\odot}$ yr^{-1}). In this regard, it is worth emphasizing that the *bad*-sBzK which are actually quenched were clearly misclassified as star forming in the first place. At the faintest B magnitudes the error δB can be so large to qualify a galaxy as a sBzK according to Equation (2), while the real B magnitude would have actually classified it as a passively evolving, pBzK galaxy. Finally, we notice that the *flattening* of the main sequence towards high masses, especially when including the *bad*-sBzK, is likely due to a large fraction of the most massive galaxies being already on their way to be quenched (e.g., Whitaker et al. 2012; C. Mancini et al., in preparation).

3.4 Radio and global near IR-to-submillimeter SED fitting

Pannella et al. (2009) and Karim et al. (2011) have measured the average SFR in various mass and redshift bins by stacking the COSMOS 1.4 GHz radio continuum emission, by using either BzK or IRAC mass-selected samples, respectively.

In Figure 7 we directly compare the results of Karim et al. (2011) with ours in the common redshift interval ($1.4 < z < 2.5$). The figure shows the SFR(UV) for sBzK-selected sources (small black points) and the stacked SFR(IR) from PACS (green filled circles) while the magenta shaded region corresponds to the radio analysis by Karim et al. (2011). To convert the average 1.4 GHz luminosities into average SFRs Karim et al. used the calibration of the radio-FIR correlation by Bell (2003). We have rescaled their data to the IMF adopted in this paper. The slope and normalization of the stacked radio SFRs are in good agreement with both the PACS ones and the UV based. This result is not surprising, given the well known tight correlation between the radio and far-IR luminosities.

An indirect approach that combines various ingredients consists in integrating the median SED of sBzK in vari-

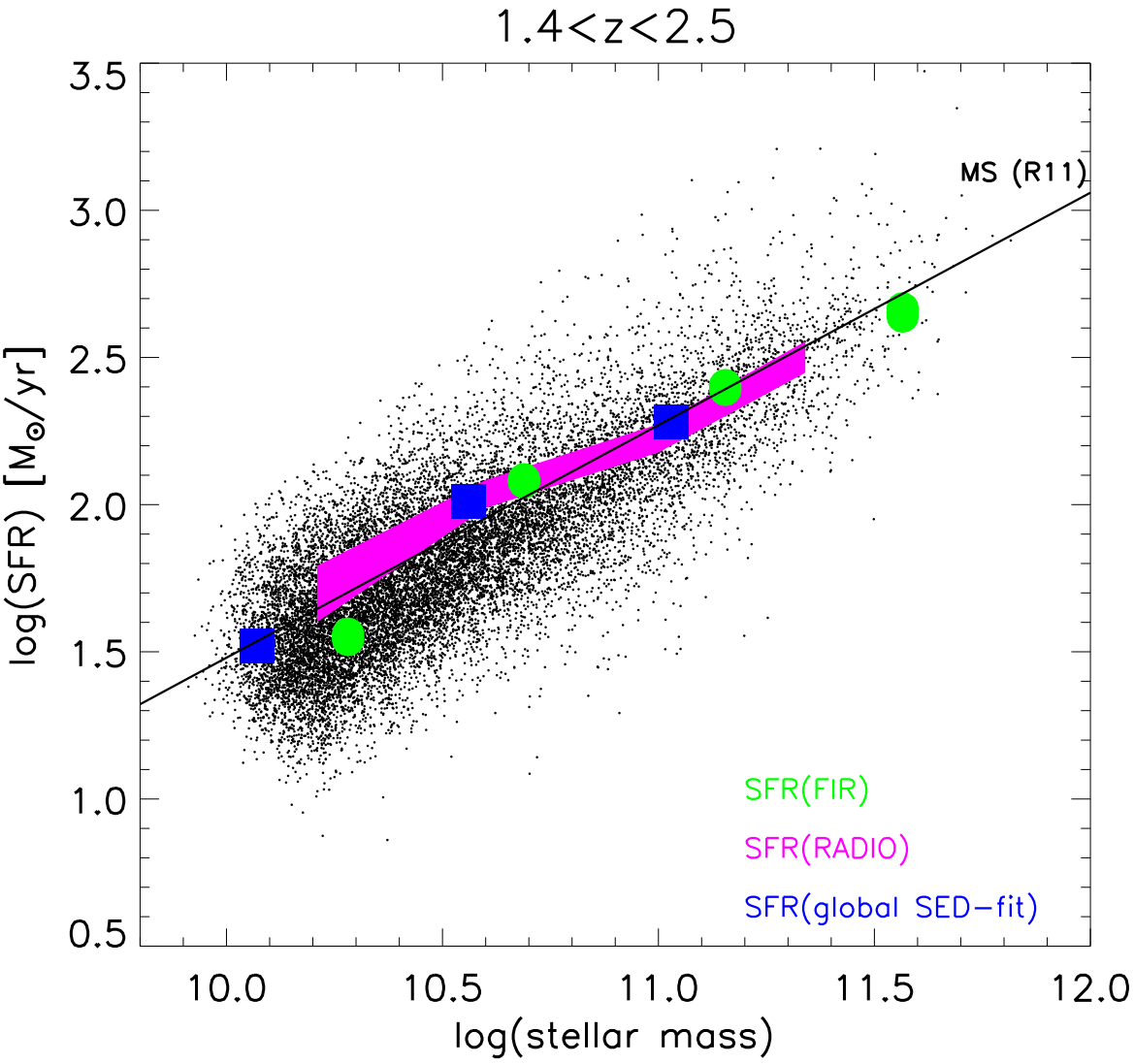

Figure 7. Comparison in the SFR-stellar mass plane of the SFR from stacked radio data (magenta shaded region, Karim et al. 2011) and stacked far-IR data (green data points, as in Figure 2 for the *good*-sBzK). We also report SFR(global SED-fit) for sBzK sources as derived in three mass bins using the median SEDs (from near-IR up to submillimeter) as derived by Magdis et al. (2012). The small black points refer to the SFR(UV) for the *good*-sBzK.

ous mass bins along the MS. As anticipated in Section 3.2, Magdis et al. (2012) have obtained average mid- to far-IR SEDs of $z \sim 2.0$ MS galaxies in three stellar mass bins, derived by stacking observed data from 16μm up to 1100μm. They also provide the total IR luminosities of each template for each mass bin, that we converted into an average SFR with Kennicutt (1998). The results of this exercise are shown as blue filled squares in Figure 7, and the resulting SFR-mass relation is fully consistent with the MS defined by UV, Herschel and radio data, providing a further support to the concordance of average SFR indicators at $z \sim 2$. It is certainly reassuring that by applying different criteria for mass-selected samples and different SFR indicators we obtain consistent results in such a wide range of stellar masses.

3.5 SFR from Hα Luminosity

As mentioned in Section 2.3, a fraction of the star-forming with photometric redshifts in the range $1.4 \lesssim z \lesssim 1.7$ have been selected as targets for the Intensive Program at the Subaru telescope with the FMOS near-IR spectrograph (J. Silverman et al. in preparation; Kashino et al. 2013). The first observing runs in the *H*-long band have provided the detection of Hα and spectroscopic redshifts for 271 galaxies, 168 of them having high quality (flag = 2) line detections. Kashino et al. include in their analysis also FMOS spectroscopy in the *J*-band, to assess the level of dust extinction by measuring the Balmer decrement using co-added spectra. They found that the extinction at Hα is an increasing function of stellar mass and they provide a linear empirical relation between these two quantities, as $A_{H\alpha} \simeq 0.60 + 1.15\,(\log[M_*/M_\odot] - 10)$. In this work we adopt this recipe

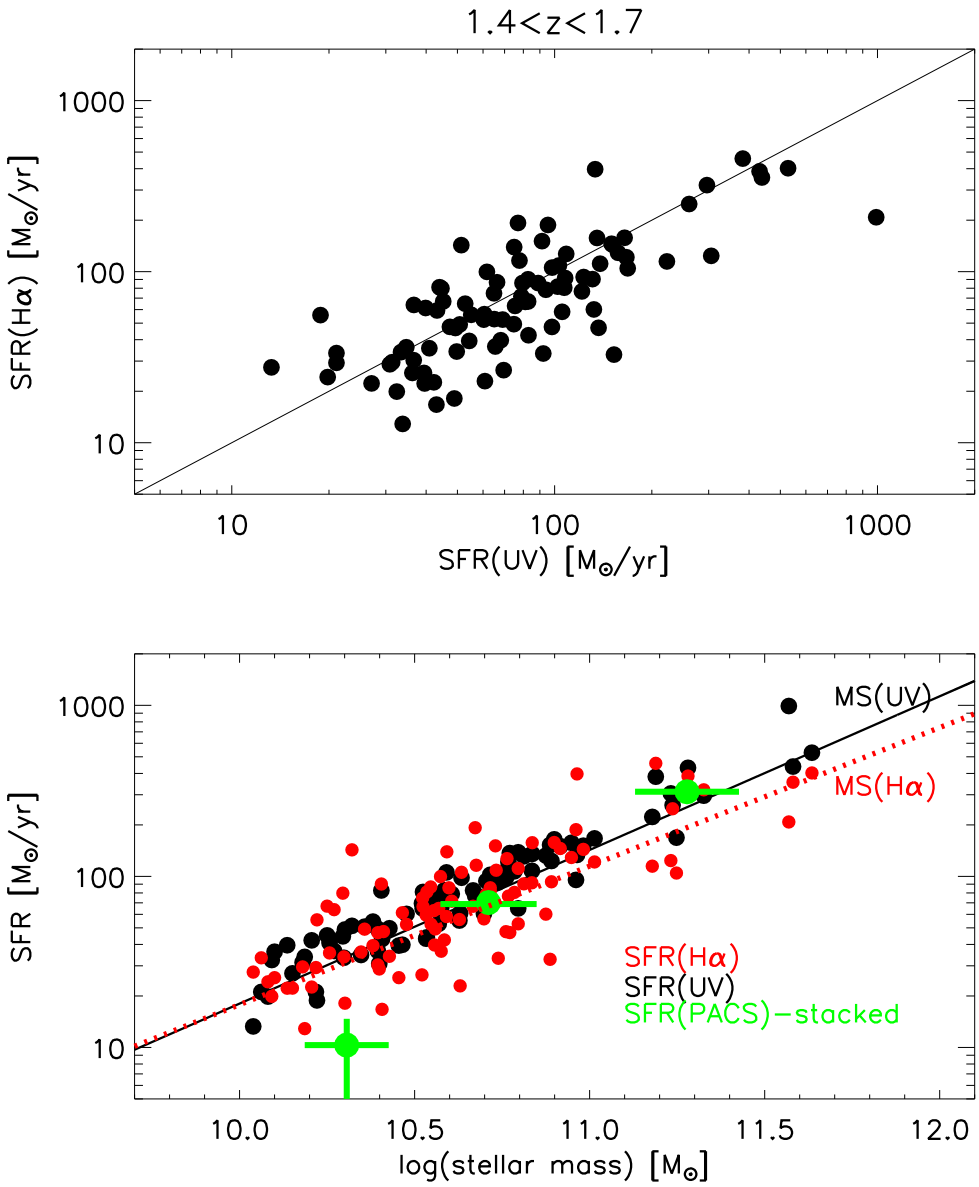

Figure 8. *Top panel:* Comparison of SFR(UV) and SFR(Hα) for a sample of sBzK sources at $1.4 < z < 1.7$ spectroscopically observed with FMOS/*Subaru* and for which a direct measure of the Hα luminosity is available (Kashino et al. 2013). Extinction corrections are derived from the average $A_{H\alpha}$-stellar mass linear relation derived by Kashino et al. (2013). *Bottom panel:* For the same sources, the stellar SFR-stellar mass relation is shown. For each source we show the SFR(UV) (black circles) and the corresponding SFR(Hα) (red circles). By stacking these sources in three mass bins on the PACS maps, we obtained a mean value of the corresponding SFR(IR) (plotted as green symbols). The width of the stacked data along the x-axis represents the standard deviation of the mass distribution in each bin. The typical uncertainties on SFR are derived by the bootstrap stacking procedure. The solid black line is the best-fit relation obtained by linear interpolation to the sBzK population with their SFR(UV) at $1.4 < z < 1.7$, while the red dotted line is the best-fit relation in the same redshift interval obtained by Kashino et al. (2013) from SFR(Hα).

to compute dust-corrected SFR(Hα) (see Section 2.3 for details), and we limit our analysis to the 168 flag=2 sources. We first compare the derived SFR(Hα) and SFR(UV) in Figure 8 (top panel), showing a good correlation between the two independent SFR measures. The median SFR(UV) for this sample is $\sim$ 20% higher than SFR(Hα), suggesting that the Balmer decrement may underestimate the total extinction (see discussion in Kashino et al. 2013). To better understand this trend, we have stacked on the 160 μm PACS maps these sources in three mass bins. This is presented in the usual mass-SFR plot in the bottom panel of Figure 8, showing for each source SFR(UV) (black circles) and the corresponding SFR(Hα) (red circles), while the green symbols show the SFR(IR) from the stacked PACS data. The width of the stacked bins along the x-axis represents the standard deviation of the mass distribution in each bin. The uncertainties on the stacked SFR are derived from the bootstrap stacking procedure, and in the two higher mass bins they are of the size of the green data points. The stacked SFR(IR) in the smaller mass bin is lower then the corre-

sponding average SFR(UV) and SFR(Hα) but we believe this is not significantly so. Contrary to the two more massive bins no individual sources are detected in the FIR and therefore the bootstrap stacking procedure underestimates the error bars. The solid black line is the MS relation obtained by linear interpolation to the sBzK population with their SFR(UV) at $1.4 < z < 1.7$ (slope $\alpha = 0.90 \pm 0.11$), while the red dotted line is the best-fit relation in the same redshift interval obtained by Kashino et al. (2013) from SFR(Hα) (slope $\alpha = 0.81 \pm 0.04$). The UV indicator is more consistent with SFR(IR) than the Hα luminosity, in particular at higher masses, where the flatter relation derived by SFR(Hα) might suggest that the extinction correction derived from the Balmer decrement is more uncertain for massive objects (cfr. Kashino et al. 2013). A slight bias is also present in the Hα sample as at low masses objects with above average SFR(UV) were selected for the FMOS observations. A more comprehensive investigation of dust extinction affecting the intrinsic luminosity of emission lines will be presented at the completion of the whole FMOS survey.

4 DISCUSSION AND CONCLUSIONS

We have used the COSMOS multiwavelength database to derive masses and star formation rates of $1.4 < z < 2.5$ galaxies using a variety of SFR indicators, such as the UV luminosity, the far-IR ($8 - 1,000$ μm) luminosity, and the 24 μm flux. For galaxies in the redshift range $1.4 < z < 1.7$ we have also estimated the SFR using the Hα line luminosity. Stellar masses have been derived from SED fits using UV-to-8μm photometry. The same set of masses have been used irrespective of the SFR indicator, so to isolate the effect of using different indicators. Of course, the characterization of high-redshift galaxies may also be biased by the specific procedure to measure stellar masses, but exploring this aspect is beyond the scope of the present paper, that is instead focused on the effects of using different SFR indicators, specifically on the slope of the SFR$-M_*$ relation followed by the majority of galaxies and known as the Main Sequence of star forming galaxies.

We have shown that the selection criteria to pick star-forming galaxies have a profound effect on the slope of the SFR-M_* relation. Using observables that are directly linked to the SFR (such as the mid- and the far-IR) the resulting SFR$-M_*$ relation tends to be essentially flat, but one recovers only a small fraction of the galaxies selected to produce a mass-limited sample. We show in particular that for $M_* \lesssim 10^{11}\, M_\odot$ the 160 μm selection (from *Herschel*) picks predominantly galaxies for which the SFR derived from the UV luminosity falls largely short of that indicated by their far-IR luminosity. Arguably, in such extreme cases this is due to the inability of the slope of the rest-frame UV continuum to estimate the true dust extinction affecting the bulk of the star formation in such galaxies. Such a selection picks predominantly starbursting outliers from the MS, but fails to pick the vast majority of star-forming galaxies in the same mass range, whose far-IR luminosities are below the *Herschel* detection limit.

To take advantage of the positive aspects represented by the reliability of far-IR based SFRs on one side, and of mass-limited samples on the other, we recour to stacking the *Herschel* data in various mass bins, showing that the logarithmic slope of the SFR$-M_*$ relation derived from such stacks is in excellent agreement with that derived from the dust-corrected UV luminosity, and is in the range $\sim 0.8-0.9$.

The considerations on the SFRs derived from the far-IR luminosity apply as well to the SFRs derived from the 24 μm flux, which actually in COSMOS reaches to lower SFR levels. This offers the opportunity to better characterize a sub-sample of star-forming sBzK-selected galaxies, i.e., those for which reddening and SFRs are poorly constrained by the observed rest-frame continuum, here nicknamed the *bad*-sBzK, i.e., those very faint in the B band. About 50% of them are detected at 24 μm and therefore qualify as star-forming galaxies. Stacking their *Herschel*/PACS 160 μm data shows they are close to the MS, though with a slightly flatter slope. However, particularly interesting are the *bad*-sBzK which are *not* detected at 24, 100 and 160 μm, and whose stacked PACS data show they have SFRs well below the MS (the blue points in Figure 5) and therefore qualify for being quenched (or quenching) galaxies. Therefore, the combination of *Herschel* with *Spitzer* data have allowed us to break the age/reddening degeneracy for sBzK-selected galaxies, thus distinguishing whether a galaxy is very red because of being heavily dust reddened, or whether it is very red because star formation has been quenched.

Finally, we have compared our SFR(UV) to the SFRs derived from the Hα luminosity of a sample of sBzK-selected galaxies at $1.4 < z < 1.7$ observed with FMOS at the Subaru telescope. The two sets of SFRs are broadly consistent with each other as they are with the SFRs derived by stacking the corresponding PACS data in two mass bins. As a result, also the SFR$-M_*$ relation using SFR(Hα) values is consistent with that derived from the other SFR indicators.

The reassuring conclusion is that a wide variety of SFR indicators, such as the rest-frame UV continuum, the mid- and the far-IR, the 1.4 GHz radio flux and the Hα luminosity all give consistent results when applied to samples as close as possible to be mass-selected samples. The slope of the main sequence can vary between ~ 0.8 and ~ 1, depending on the specific selection criterion and on the adopted SFR indicator, which all must introduce a small bias. Perhaps the most intriguing of such biases comes from how star-forming galaxies are identified as such, as especially at high masses a non trivial fraction (almost $\sim 15\%$)) of sBzK-selected galaxies (selected for being star forming) turns out to be already quenched or well on their way to be quenched, as indeed expected to happen thanks to the *mass quenching* process, an effect that tends to flatten the slope of the main sequence. Ironically, many *bad*-sBzK with low SFR(UV) turn out to be very powerful mid- and far-IR sources and are starbursting MS outliers.

ACKNOWLEDGMENTS

GR, IB and AF acknowledge support from the University of Padova from ASI (Herschel Science Contract I/005/07/0). AR acknowledges funding support from a INAF-PRIN-2010 grant. ED acknowledges funding support from ERC-StG grant UPGAL 240039 and ANR-08-JCJC-0008. GC acknowledges support from grant PRIN-INAF 2011 "Black hole growth and AGN feedback through the cosmic time

AC acknowledges the MIUR PRIN 2010-2011 "The dark Universe and the cosmic evolution of baryons: from current surveys to Euclid". This work was supported by World Premier International Research Center Initiative (WPI Initiative), MEXT, Japan.

PACS has been developed by a consortium of institutes led by MPE (Germany) and including UVIE (Austria); KU Leuven, CSL, IMEC (Belgium); CEA, LAM (France); MPIA (Germany); INAF- IFSI/OAA/OAP/OAT, LENS, SISSA (Italy); IAC (Spain). This development has been supported by the funding agencies BMVIT (Austria), ESA-PRODEX (Belgium), CEA/CNES (France), DLR (Germany), ASI/INAF (Italy), and CICYT/MCYT (Spain).

We thank the anonymous referee for a careful reading and valuable comments, which have significantly contributed to improve the clarity of the paper.

REFERENCES

Bell, E. F. 2003, ApJ, 586, 794
Berta, S., Lutz, D., Santini, P., et al. 2013, A&A, 551, A100
Béthermin, M., Dole, H., Beelen, A., & Aussel, H. 2010, A&A, 512, A78
Brinchmann, J., Charlot, S., White, S. D. M., Tremonti, C., Kauffmann, G., Heckman, T., & Brinkmann, J. 2004, MNRAS, 351, 1151
Chary, R., & Elbaz, D. 2001, ApJ, 556, 562
Cresci, G., Hicks, E. K. S., Genzel, R., et al. 2009, ApJ, 697, 115
Daddi, E., Cimatti, A., Renzini, A. et al. 2004, ApJ, 617, 746
Daddi, E., Renzini, A., Pirzkal, N. et al. 2005, ApJL, 631, L13
Daddi, E., Dickinson, M., Morrison, G. et al. 2007, ApJ, 670, 156
Di Matteo, P., Bournaud, F., Martig, M., Combes, F., Melchior, A.-L., & Semelin, B. 2008, A&A, 492, 31
Domínguez Sánchez, H., Mignoli, M., Pozzi, F., et al. 2012, MNRAS, 426, 330
Elbaz, D., Daddi, E., Le Borgne, D. et al. 2007, A&A, 468, 33
Elbaz, D., Dickinson, M., Hwang, H. S. et al. 2011, A&A, 533, A.119
Erb, D. K., Steidel, C. C., Shapley, A. E., et al. 2006, ApJ, 647, 128
Förster Schreiber, N. M., Genzel, R., Bouché, N., et al. 2009, ApJ, 706, 1364
Ilbert, O., Salvato, M., Le Floc'h, E. et al. 2010, ApJ, 709, 644
Karim, A., Schinnerer, E., Martinez-Sansigre, A. 2011, ApJ, 730, 61
Kashino, D., Silverman, J. D., Rodighiero, G., et al. 2013, ApJL, 777, L8
Kennicutt, R. C., Jr. 1998, ARA&A, 36, 189
Law, D. R., Steidel, C. C., Erb, D. K., et al. 2009, ApJ, 697, 2057
Lilly, S. J., Carollo, C. M., Pipino, A., Renzini, A., & Peng, Y. 2013, ApJ, 772, 119
Lutz, D., Poglitsch, A., Altieri, B. et al. 2011, A&A, 532, A90
Magdis, G. E., Daddi, E., Bthermin, M. et al. 2012, ApJ, 760, 6
Magnelli, B., Elbaz, D., Chary, R. R., et al. 2009, A&A, 496, 57
Maraston, C., Pforr, J., Renzini, A., et al. 2010, MNRAS, 407, 830
McCracken, H. J., Capak, P., Salvato, M. et al. 2010, ApJ, 708, 202
Noeske, K. G., Weiner, B. J., Faber, S. M. et al. 2007, ApJL, 660, L43
Nordon, R., Lutz, D., Shao, L. et al. 2010, A&A, 518, L24
Nordon, R., Lutz, D., Genzel, R., et al. 2012, ApJ, 745, 182
Pannella, M., Carilli, C. L., Daddi, E. et al. 2009, ApJL, 698, L116
Peng, Y.-j., Lilly, S.J., Kovac, K. et al. 2010, ApJ, 721, 193
Peng, Y.-j., Lilly, S.J., Renzini, A., & Carollo, C.M. 2013, ApJ, submitted
Popesso, P., Magnelli, B., Buttiglione, S., et al. 2012, arXiv:1211.4257
Reddy, N. A., Steidel, C. C., Fadda, D., Yan, L., Pettini, M., Shapley, A. E., Erb, D. K., & Adelberger, K. L. 2006, ApJ, 644, 792
Reddy, N., Dickinson, M., Elbaz, D. et al. 2012, ApJ, 744, 154
Renzini, A. 2009, MNRAS, 398, L58
Rodighiero, G., Vaccari, M., Franceschini, A. et al. 2010a, A&A, 515, A8
Rodighiero, G., Cimatti, A., Gruppioni, C. et al. 2010b, A&A, 518, L25
Rodighiero, G., Daddi, E., Baronchelli, I. et al. 2011, ApJ, 739, L40
Salpeter, E. E. 1955, ApJ, 121, 161
Sanders, D. B., Soifer, B. T., Elias, J. H., Madore, B. F., Matthews, K., Neugebauer, G., & Scoville, N. Z. 1988, ApJ, 325, 74
Santini, P., Fontana, A., Grazian, A., et al. 2009, A&A, 504, 751
Scoville, N., Aussel, H., Brusa, M. et al. 2007, ApJS, 172, 1
Whitaker, K.E., van Dokkum, P.G., Brammer, G. & Franx, M. 2012, ApJ, 754, L29
Wuyts, S., Förster Schreiber, N.M., van der Wel, A. et al. 2011, ApJ, 742, 96
Zahid, H.J., Kashinom D., Silverman, J.D. et al. 2013, arXiv/1310.4950